STATE-OF-CHARGE ESTIMATION FOR SUPERCAPACITORS: A KALMAN FILTERING FORMULATION

Andrew Nadeau, Gaurav Sharma, Tolga Soyata

University of Rochester, Dept. of Electrical and Computer Engineering, Rochester, NY 14627
{andrew.nadeau, gaurav.sharma, tolga.soyata}@rochester.edu

ABSTRACT

Supercapacitors are an attractive option for energy buffering because of their high efficiency, durability, and low environmental impact. For energy-aware applications, it is desirable to accurately estimate the buffered energy. Under conditions of varying energy supply and demand, estimation of buffered energy by using only the supercapacitor terminal voltage is inaccurate because this does not fully comprehend the physical *state of charge*. To address this problem, we present a Kalman filtering formulation, using the accepted three-branch circuit model for supercapacitors. Compared with an ideal capacitor, the physically-motivated three-branch model provides a much more accurate representation of the *state of charge* via three internal state voltages associated with short, medium, and long term charging constants. The proposed Kalman formulation tracks these unobservable internal states. This methodology demonstrates a significantly more accurate estimate of the buffered energy as compared with the alternative models of ideal capacitance or a recursive computation of the stored energy. Simulations conducted with variations that approximate recorded solar intensity profiles, our proposed approach has an error of 1% compared with 31% and 85% for the respective alternative models.

Index Terms— supercapacitor, ultracapacitor, electric double layer capacitor, solar energy, kalman filter, state of charge, energy awareness.

1. INTRODUCTION

Supercapacitors are established as a compelling solution for high power buffering applications. These applications favor supercapacitors due to their ability to bank and supply power at levels an order of magnitude beyond the capabilities of electrochemical battery technologies per unit weight. This superior power density has been utilized for regenerative breaking [1], elevator [2], and automating starting systems for combustion engines [3]. Supercapacitors can also provide sufficient energy density (e.g., Maxwell 3000F [4] with a storage capacity of 11,000 Joules) for deployment in field sys-

tems demanding much lower power consumption levels (e.g., 10 mW–10 W [5, 6]). For these systems, where energy is at a premium, being able to predict the remaining energy (i.e., time-to-full-depletion) plays an extremely important role for operational efficiency. Although the remaining supercapacitor energy can be naïvely predicted as $E = \frac{1}{2}CV^2$, this is far from accurate for systems where the range of operational power consumption is wide (e.g., two orders-of-magnitude). This fact is due to the non-ideal behavior of supercapacitors, modeled in [7, 8, 9]. Due to the electrochemical make-up of the supercapacitors, significant electrical and chemical phenomena effect its response, thereby creating unobservable internal states of charge.

In this paper, we describe a model which treats these internal states as unobservable variables, as well as the supercapacitor current and voltage as the controllable input and observable output, respectively. By using a extended Kalman filter (EKF), the internal states are continuously estimated and updated based on the observed input voltage/current. Our simulations, implementing the three branch equivalent circuit model [9], demonstrate an improved energy estimation accuracy from 31% to 1%. The remainder of this paper is organized as follows: In Section 2, background information is provided on supercapacitor modeling. An introduction to the EKF and our modeling of the supercapacitor to allow Kalman filtering for internal state estimation are provided in Section 3. Naïve estimation-based as well as our Kalman-based simulation results are provided in Section 4, followed by our conclusions and future directions in Section 5.

2. SUPERCAPACITOR MODELING

Compared to electrolytic capacitors, supercapacitors provide significantly higher capacitance. This higher capacitance is obtained by having porous, activated carbon electrodes with a very large effective surface area, and enables kilo-Farad level capacitances to be packaged in hand-held form factors. At the same time, however, when supercapacitors are charged or discharged, the charge from the terminal takes significantly different amounts of time to migrate through the porous surfaces to or from the different regions of the electrode area. As a result, under rapid charging or discharging, charge buildup
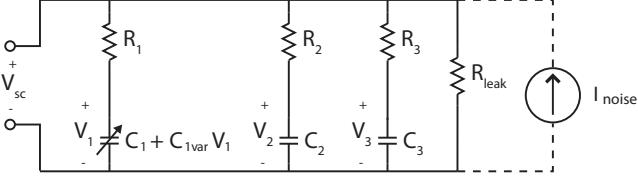
Fig. 1. Three-branch supercapacitor equivalent circuit [9].

in different regions of the electrode area is not homogeneous and charge re-distribution side effects are encountered. After the current stops after a period of rapid discharging, terminal voltage rebounds as charge "redistributes" from deeper pores. Vice versa, after rapid charging, charge redistribution causes a fall in terminal voltage. Leakage can also impact how much usable energy remains in a supercapacitor, but this long term effect can be insignificant for the time frame of charge redistribution [7, 8]. Because of charge redistribution, terminal voltage is insufficient to measure supercapacitors' state of charge (SOC).

Diffusion through the porous electrode can be precisely modeled using series RC-transmission line representation [10]. The distributed transmission line model is, however, intractable to work with and therefore a simplified three-branch model shown in Fig. 1, which accounts for charge redistribution with just three parallel RC-branches, has been proposed [9]. The model is much more tractable because it uses only lumped circuit elements and has been shown to be effective in modeling SOC, when used with parameter values estimated for the R and C elements from experimentally measured device data [9].

Using the three branch model in Fig. 1, this paper presents an extended Kalman filter (EKF) approach for tracking the buffered energy in a supercapacitor. The EKF uses the internal voltages across the capacitances in each of the three branches to represent the SOC. Because these voltages are not directly observable the EKF is needed to track them. Our approach shares some similarities with prior work on the SOC observability problem for battery systems, where Kalman filtering is a widely implemented solution [11, 12, 13]. The device models are very different in the two scenarios and so are the Kalman filter formulations.

3. EXTENDED KALMAN FILTER

The EKF tracks the hidden SOC in the three-branch supercapacitor model using recursive **predict** and **update** operations. For each time interval Δt_k, the EKF predicts the current SOC, $\mathbf{x}_k = [V_1 \quad V_2 \quad V_3]^{\mathrm{T}}$, and terminal voltage $\mathbf{z}_k = V_{\mathrm{sc}}$:

$$\tilde{\mathbf{x}}_k = f_k(\hat{\mathbf{x}}_{k-1}, \mathbf{u}_{k-1}, \Delta t_k). \qquad (1)$$

$$\tilde{\mathbf{z}}_k = h_k(\tilde{\mathbf{x}}_k, \mathbf{u}_k). \qquad (2)$$

The predictions $\tilde{\mathbf{x}}_k$ and $\tilde{\mathbf{z}}_k$ depend on the input current, $\mathbf{u}_{k-1} = I_{\mathrm{sc}}$, and previous estimate, $\hat{\mathbf{x}}_{k-1}$. $\tilde{\mathbf{x}}_k$ is updated to

incorporate new information from the observation $\mathbf{z}_k$, according to the Kalman gain matrix [14, 15], $\mathbf{K}_k$:

$$\hat{\mathbf{x}}_k = \tilde{\mathbf{x}}_k + \mathbf{K}_k (\mathbf{z}_k - \tilde{\mathbf{z}}_k), \qquad (3)$$

$\mathbf{K}_k$ balances between **predict** and **update** by treating uncertainty in each as normally distributed random variables, and tracking their respective covariance matrices, $\tilde{\mathbf{P}}_k$, and $\tilde{\mathbf{S}}_k$. This allows whichever has lower uncertainty to be favored.

The critical EKF implementation details are: *a*) evaluating the prediction and update operations, and *b*) modelling uncertainty with the covariances $\tilde{\mathbf{P}}_k$, and $\tilde{\mathbf{S}}_k$ to achieve acceptable balance in $\mathbf{K}_k$.

The prediction functions f and h, are numerically evaluated using the system of differential equations from the equivalent circuit in Fig. 1, viz.,

$$\frac{d}{dt}\mathbf{x} = \mathbf{F}_k\mathbf{x} + \mathbf{B}_k\mathbf{u}, \qquad (4)$$

$$\mathbf{z} = \mathbf{H}_k\mathbf{x} + \mathbf{D}_k\mathbf{u}. \qquad (5)$$

where the matrices $\mathbf{F}_k$, $\mathbf{H}_k$, $\mathbf{B}_k$, and $\mathbf{D}_k$ can be obtained in terms of the values for the circuit elements in Fig. 1 as summarized in the equations listed at the top of the next page (in two column format). The numeric solver produces $\tilde{\mathbf{x}}_k$ and $\tilde{\mathbf{z}}_k$ from (4) and (5) using the time interval Δt_k and initial conditions $\hat{\mathbf{x}}_{k-1}$.

Balancing the Kalman gain (matrix) $\mathbf{K}_k$ between predictions from an approximate model, and observations that may be noisy or incomplete, is difficult. Disregarding uncertainty allows exact prediction via solution of the equivalent circuit. However, without modeled uncertainty, $\tilde{\mathbf{P}}_k$, and $\tilde{\mathbf{S}}_k$ decrease each iteration, eventually leaving $\mathbf{K}_k$ undefined.

Our EKF models uncertainty using the additional unobserved noise current, I_{noise} in Fig. 1. I_{noise} is a random, zero mean signal with bandwidth and power proportional to $\mathbf{u}_k$. I_{noise} can be accurately modelled by the process and observation noise covariances, $\mathbf{Q}_k$ and $\mathbf{R}_k$, in the EKF first-order approximation[1]:

$$\mathbf{x}_k \approx \mathbf{x}_{k-1} + (\mathbf{F}\mathbf{x}_{k-1} + \mathbf{B}\mathbf{u}_{k-1})\,\Delta t_k + \mathcal{N}(0, \mathbf{Q}_k), \quad (6)$$

$$\mathbf{z}_k \approx \mathbf{H}\mathbf{x}_k + \mathbf{D}\mathbf{u}_k + \mathcal{N}(0, \mathbf{R}_k). \qquad (7)$$

$\mathbf{Q}_k$ and $\mathbf{R}_k$ are then used to calculate the Kalman gain:

$$\tilde{\mathbf{P}}_k = (\mathbf{I} + \mathbf{F}_k)\,\hat{\mathbf{P}}_{k-1}\,(\mathbf{I} + \mathbf{F}_k)^{\mathrm{T}} + \mathbf{Q}_k, \qquad (8)$$

$$\tilde{\mathbf{S}}_k = \mathbf{H}_k\tilde{\mathbf{P}}_k\mathbf{H}_k^{\mathrm{T}} + \mathbf{R}_k, \qquad (9)$$

$$\mathbf{K}_k = \tilde{\mathbf{P}}_k\mathbf{H}_k^{\mathrm{T}}\tilde{\mathbf{S}}_k^{-1}. \qquad (10)$$

The intuition behind calculating $\mathbf{Q}_k$ and $\mathbf{R}_k$ from I_{noise} is: **uncertainty should be proportional to the rate-of-change of the individual internal states**. Slowly charging

---

[1]The UKF (unscented Kalman filter) can improve the accuracy of propagating uncertainty $\hat{\mathbf{P}}_k$ through the model [16, 12], but does not address how to characterize process noise as the Gaussian process, $\mathcal{N}(0, \mathbf{Q}_k)$. Because $\mathbf{x}_k$ represents capacitor voltages which are continuous in time, linear EKF approximations are adequate.

$$\mathbf{F}_k = \begin{bmatrix} \frac{1}{R_1 C_1'}\left(\frac{R_\parallel}{R_1}-1\right) & \frac{1}{R_1 C_1'}\frac{R_\parallel}{R_2} & \frac{1}{R_1 C_1'}\frac{R_\parallel}{R_2} \\ \frac{1}{R_2 C_2}\frac{R_\parallel}{R_1} & \frac{1}{R_2 C_2}\left(\frac{R_\parallel}{R_2}-1\right) & \frac{1}{R_2 C_2}\frac{R_\parallel}{R_2} \\ \frac{1}{R_3 C_3}\frac{R_\parallel}{R_1} & \frac{1}{R_3 C_3}\frac{R_\parallel}{R_2} & \frac{1}{R_3 C_3}\left(\frac{R_\parallel}{R_2}-1\right) \end{bmatrix}, \quad \mathbf{B}_k = \begin{bmatrix} \frac{1}{R_1 C_1'}R_\parallel \\ \frac{1}{R_2 C_2}R_\parallel \\ \frac{1}{R_3 C_3}R_\parallel \end{bmatrix}, \quad \left| \quad R_\parallel = R_1\|R_2\|R_3\|R_{\text{leak}}, \right.$$

$$\mathbf{H}_k = \begin{bmatrix} \frac{R_\parallel}{R_1} & \frac{R_\parallel}{R_2} & \frac{R_\parallel}{R_3} \end{bmatrix}, \qquad\qquad\qquad \mathbf{D}_k = \begin{bmatrix} R_\parallel \end{bmatrix}, \quad \left| \quad C_1' = C_1 + C_{1\text{var}}\, V_1|_k. \right.$$

(small $\mathbf{u}_k$), decreases the bandwidth of I_{noise}, penetrating all three branches (low-pass filters) regardless of time-constant. Hence, uncertainty in all branches allows predictions of V_2 and V_3 to be updated when voltage settles and branch voltages are most apparent from the observation. Quickly charging (large $\mathbf{u}_k$), increases the bandwidth, decreasing prediction uncertainty for branches that do not react to abrupt charging.

Formulating $\mathbf{Q}_k$ and $\mathbf{R}_k$ from the continuous random I_{noise} signal is done by applying the linear approximation (6) recursively to the noise signal N times within the interval Δt_k:

$$\mathcal{N}(0, \mathbf{Q}_k) = \sum_{n=1}^{N} \left(\mathbf{I} + \mathbf{F}\tfrac{\Delta t_k}{N}\right)^{n-1} \mathbf{B}\tfrac{\Delta t_k}{N}\, I_{\text{noise}}|_{n-1}. \quad (11)$$

Because (11) is a weighted sum of the normally distributed values of I_{noise}, finding the covariance $\mathbf{Q}_k$ is straightforward. The output covariance $\mathbf{R}_k$ is determined by the value $I_{\text{noise},N}$ when $\mathbf{z}_k$ is observed, and is uncorrelated with the process noise:

$$\mathcal{N}(0, \mathbf{R}_k) = \mathbf{D}I_{\text{noise},N}. \quad (12)$$

4. EVALUATION

For evaluating our proposed framework we used the three-branch model for two devices: a 1500F supercapacitor whose parameters were reported in [9] and a 50F supercapacitor for which we measured parameters in our lab, following the protocol recommended in [9]. Both sets of parameters are listed in Table 1. These devices have a rated voltage of 2.7V and for evaluating SOC tracking performance, we consider a charging profile motivated by a solar harvesting application. Measured solar variability, and corresponding power variation that must be buffered by the supercapacitor are shown in Fig. 4. Figure 4 demonstrates a two decade dynamic range for power availability in solar harvesting. To simplify the evaluation of SOC tracking performance under such variability, we consider a synthetic profile for the input charging current I_{sc} that is shown in Fig. 2(a), where the current profile is designed to test SOC tracking by repeatedly charging and discharging the supercapcitor between 0V and its rated voltage 2.7V at decreasing rates each cycle. Average power for each cycle is annotated on the voltage output in Fig. 2(b). The logarithmic scale allows Fig. 2 to show very fast charging ($\sim$1 minute) initially, with progressively slower charges (up to $\sim$9 hours) on the same axes. Using the logarithmic scale, the corresponding

	Maxwell 50F BCAP (measured)	1500F DLC (ref. [9])
C_{rated}	50F	1500F
C_1	42.5F	900F
C_{1var}	$5.1\frac{F}{V}$	$600\frac{F}{V}$
R_1	16 mΩ	1.5 mΩ
C_2	10.5F	200F
R_2	112 Ω	400 mΩ
C_3	4F	330F
R_3	628Ω	3.2Ω
R_{leak}	36kΩ	4kΩ

Table 1. Parameters for the three branch model.

solar power variability region is plotted in Fig. 2(b) for the 1500F capacitor. Doubling the solar array size or halving the capacitance for the system shifts the *solar power variability region* left, while opposite changes push it right into the more benign supercapacitor power levels.

The wide range of powers applied to the supercapacitor bring out the relevance of the three-branch internal state, especially for the initial high power cycles that cause the internal states, V_2 and V_3 to deviate significantly from the observed voltage. For low power cycles, internal states remain very close to the observed terminal voltage and the observability problem motivating the EKF is not as significant. This is the situation for low power sensor node applications [17], for instance.

EKF iterative SOC estimations are shown as points in Fig. 2(b), and separated by $\Delta t_k \propto I_{\text{sc}}$ such that change in V_{sc} each iteration is approximately 10% of the rated voltage. Sampling rate $\frac{N}{\Delta t_k}$, for the I_{noise} signal is also proportional to I_{sc}:

$$T_{\text{charge}}(k) \approx (1500\text{F})(2.7\text{V}) \div I_{\text{sc}}|_k = 10\Delta t_k = 40\tfrac{\Delta t_k}{N} \quad (13)$$

Ground truth for the supercapacitor behavior shown in Fig. 2 is generated using Simulink to provide truth data for three-branch internal states that cannot be accessed in physical devices. Parameters given in Table 1, measured from a 1500F supercapacitor are used to calibrate the simulation. I_{sc} and I_{noise} sum together to produce the input current to the reference simulation. I_{noise} models uncertainty and is randomly generated such that $20\log_{10}\left|\frac{I_{\text{sc}}}{\sigma_{\text{noise}}}\right| = 20$dB.

Accuracy for four energy-accounting schemes is shown in Fig. 3. The first is a recursive "Coulomb count" technique that tracks energy by integrating net power over each time interval.
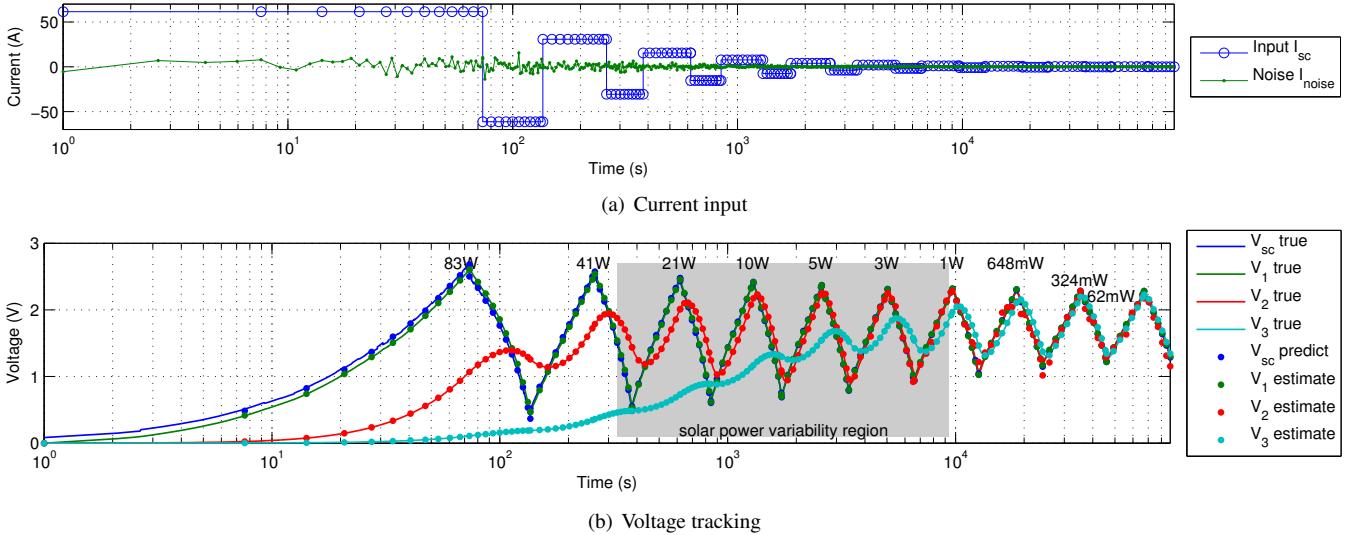
(a) Current input

(b) Voltage tracking

Fig. 2. The current (a), and voltage (b) charge-discharge profiles tests EKF state tracking over a range of power levels. The logarithmic scale shows cycles ranging from in duration from $\sim$1minute to $\sim$ 9 hours.

Integrating fails to account for internal losses in the supercapacitor and allows error from unobserved I_{noise} to accumulate, especially at high power levels. The second method, estimates energy using the idealized capacitor model of "$^1/_2 C V_{\text{sc}}^2$". Because V_{sc} is observed, error does not accumulate, but there is significant error because the dynamics of the three-branch model are ignored in this over-simplification. The third and final "predict only" technique models the true three-branch dynamics, but sets $\mathbf{K}_k$ to zero throughout, disregarding V_{sc} observations. This provides the best accuracy among methods other than the EKF, but still allows error to accumulate. The EKF "Kalman" provides the best accuracy by accounting for the true three-branch dynamics of the internal SOC and also the uncertainty associated with observations.

5. CONCLUSIONS

The naïve remaining energy formula of $E = \frac{1}{2} C V^2$ yields inaccurate results for the energy stored in a supercapacitor, especially when the power consumption range of the supercapacitor-based system is wide (two or more orders of magnitude). This formula, which is suitable for a regular capacitor proves inaccurate because the physical phenomena associated with supercapacitor charging create unobservable internal states of charge (SOC).

A Kalman Filter-based method is introduced to continuously predict and estimate the internal states by sampling the supercapacitor terminal voltage and current, which are the only two observable values. The methodology is validated via simulations using a synthetic charge-discharge profile that spans measured dynamic range in solar power variation. Results indicate that the proposed approach significantly improves the estimates of available energy, attaining root mean squared error of 1% compared to 31% for the naïve $E = \frac{1}{2} C V^2$ model.
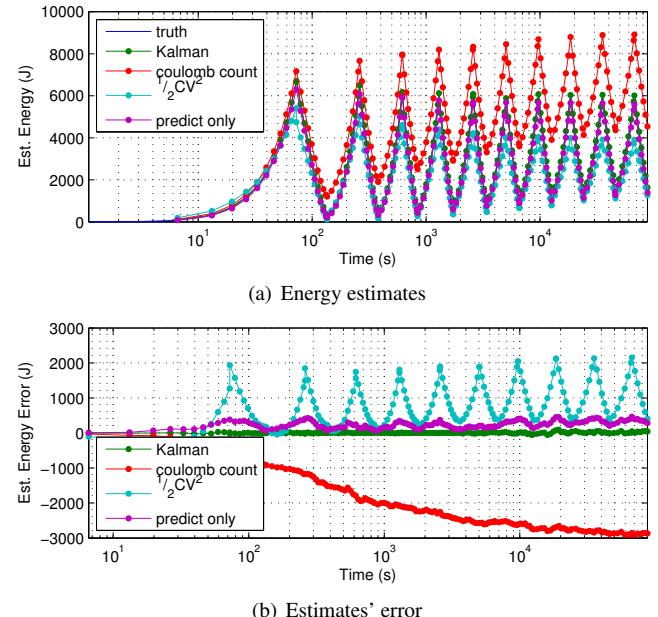

(a) Energy estimates

(b) Estimates' error

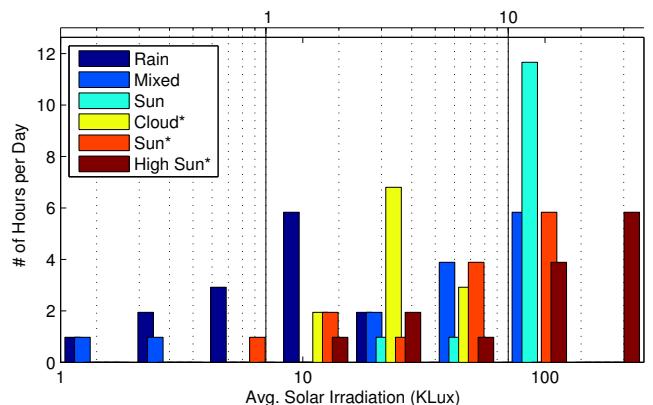**Fig. 3**. Comparison of the accuracy of energy-awareness methods

Fig. 4. Solar power from 21 pannels (max. 25.5W) varies by two orders-of-magnitude. Marked data (*) is taken from [18].

6. REFERENCES

[1] D. Rotenberg, A. Vahidi, and I. Kolmanovsky, "Ultracapacitor assisted powertrains: Modeling, control, sizing, and the impact on fuel economy," *IEEE Trans. Control Syst. Technol.*, vol. 19, no. 3, pp. 576–589, 2011.

[2] A. Rufer and P. Barrade, "A supercapacitor-based energy storage system for elevators with soft commutated interface," *IEEE Trans. Ind. Appl.*, vol. 38, no. 5, pp. 1151–1159, 2002.

[3] H. A. Catherino, J. F. Burgel, P. L. Shi, A. Rusek, and X. Zou, "Hybrid power supplies: A capacitor-assisted battery," *J. of Power Sources*, vol. 162, no. 2, pp. 965 – 970, 2006. [Online]. Available: http://www.sciencedirect.com/science/article/pii/S0378775305008748

[4] Maxwell Corp., "K2 Series High Capacity Cells," http://www.maxwell.com/products/ultracapacitors/products/k2-series, 2012.

[5] A. Fahad, T. Soyata, T. Wang, G. Sharma, W. Heinzelman, and K. Shen, "SOLARCAP: super capacitor buffering of solar energy for self-sustainable field systems," in *Proc. of the 25th IEEE Intl. System-on-Chip Conf.*, Niagara Falls, NY, Sep 2012, pp. 236–241.

[6] D. Brunelli, L. Benini, C. Moser, and L. Thiele, "An efficient solar energy harvester for wireless sensor nodes," in *Conf. on Design, Automation and Test in Europe (DATE)*, Munich, Germany, Mar. 2008, pp. 104–109.

[7] Y. Zhang and H. Yang, "Modeling and characterization of supercapacitors for wireless sensor network applications," *J. Power Sources*, vol. 196, no. 8, pp. 4128–4135, 2011. [Online]. Available: http://www.sciencedirect.com/science/article/pii/S0378775310021440

[8] H. Yang and Y. Zhang, "Self-discharge analysis and characterization of supercapacitors for environmentally powered wireless sensor network applications," *J. Power Sources*, vol. 196, no. 20, pp. 8866–8873, 2011. [Online]. Available: http://www.sciencedirect.com/science/article/pii/S0378775311012237

[9] L. Zubieta and R. Bonert, "Characterization of double-layer capacitors for power electronics applications," *IEEE Trans. Ind. Appl.*, vol. 36, no. 1, pp. 199–205, 2000.

[10] N. Bertrand, J. Sabatier, O. Briat, and J.-M. Vinassa, "Embedded fractional nonlinear supercapacitor model and its parametric estimation method," *IEEE Trans. Ind. Appl.*, vol. 57, no. 12, pp. 3991–4000, 2010.

[11] B. S. Bhangu, P. Bentley, D. A. Stone, and C. M. Bingham, "Nonlinear observers for predicting state-of-charge and state-of-health of lead-acid batteries for hybrid-electric vehicles," *IEEE Trans. Veh. Technol.*, vol. 54, no. 3, pp. 783–794, 2005.

[12] G. L. Plett, "Sigma-point Kalman filtering for battery management systems of LiPB-based HEV battery packs: Part 1: Introduction and state estimation," *J. Power Sources*, vol. 161, no. 2, pp. 1356–1368, 2006.

[13] ——, "Extended Kalman filtering for battery management systems of LiPB-based HEV battery packs: Part 3. State and parameter estimation," *J. Power Sources*, vol. 134, no. 2, pp. 277–292, 2004. [Online]. Available: http://www.sciencedirect.com/science/article/pii/S0378775304003611

[14] S. Haykin, *Adaptive Filter Theory*. Prentice Hall, 2002.

[15] G. L. Plett, "Extended Kalman filtering for battery management systems of LiPB-based HEV battery packs: Part 1. background," *J. Power Sources*, vol. 134, no. 2, pp. 252–261, 2004. [Online]. Available: http://www.sciencedirect.com/science/article/pii/S0378775304003593

[16] R. Van der Merwe and E. A. Wan, "The square-root unscented Kalman filter for state and parameter-estimation," in *Proc. IEEE Intl. Conf. on Acoustics, Speech, and Sig, Proc. (ICASSP)*, vol. 6, 2001, pp. 3461–3464.

[17] C. Renner and V. Turau, "State-of-charge assessment for supercap-powered sensor nodes: Keep it simple stupid!" in *IEEE Ninth Intl. Conf. on Networked Sensing Systems (INSS)*, 2012, pp. 1–6.

[18] R. Faranda and S. Leva, "Energy comparison of MPPT techniques for PV systems," *WSEAS Trans. on Power Systems*, vol. 3, no. 6, pp. 446–455, 2008.